J. Fluid Mech. (2022), *vol*. 932, A10, doi:10.1017/jfm.2021.978

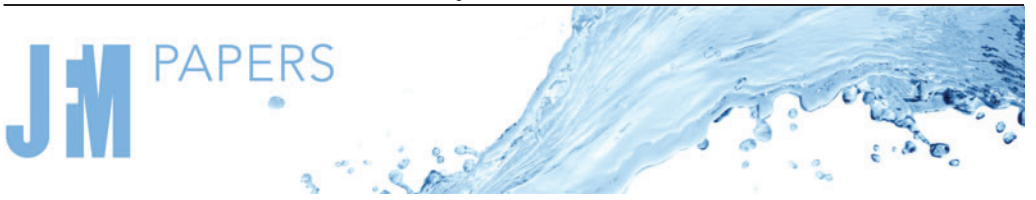

Navigation of micro-swimmers in steady flow: the importance of symmetries

Jingran Qiu[1], Navid Mousavi[2], Kristian Gustavsson[2], Chunxiao Xu[1], Bernhard Mehlig[2] and Lihao Zhao[1],†

[1]AML, Department of Engineering Mechanics, Tsinghua University, 100084 Beijing, PR China

[2]Department of Physics, University of Gothenburg, SE-41296 Gothenburg, Sweden

(Received 19 April 2021; revised 20 October 2021; accepted 29 October 2021)

Marine micro-organisms must cope with complex flow patterns and even turbulence as they navigate the ocean. To survive they must avoid predation and find efficient energy sources. A major difficulty in analysing possible survival strategies is that the time series of environmental cues in nonlinear flow is complex and that it depends on the decisions taken by the organism. One way of determining and evaluating optimal strategies is reinforcement learning. In a proof-of-principle study, Colabrese *et al.* (*Phys. Rev. Lett.*, vol. 118, 2017, 158004) used this method to find out how a micro-swimmer in a vortex flow can navigate towards the surface as quickly as possible, given a fixed swimming speed. The swimmer measured its instantaneous swimming direction and the local flow vorticity in the laboratory frame, and reacted to these cues by swimming either left, right, up or down. However, usually a motile micro-organism measures the local flow rather than global information, and it can only react in relation to the local flow because, in general, it cannot access global information (such as up or down in the laboratory frame). Here we analyse optimal strategies with local signals and actions that do not refer to the laboratory frame. We demonstrate that symmetry breaking is required to find such strategies. Using reinforcement learning, we analyse the emerging strategies for different sets of environmental cues that micro-organisms are known to measure.

Key words: micro-organism dynamics, active matter, machine learning

1. Introduction

Active micro-organisms are ubiquitous in marine environments. They can adjust their motion in response to hydrodynamic signals. It is thought micro-organisms evolved these mechanisms to survive in the ocean. For example, when planktonic copepods or protists sense strong fluid strains, they jump (Kiørboe & Visser 1999) or change their

† Email address for correspondence: zhaolihao@mail.tsinghua.edu.cn

swimming direction (Jakobsen 2001) to avoid potential predators or to attack prey. To avoid wind-induced water turbulence near the ocean surface, marine micro-organisms migrate downwards, in response to turbulent strains, and return to the surface after the turbulence subsides (Incze *et al.* 2001; Maar *et al.* 2006). In this case, the actions are less vigorous, involving smaller accelerations. Copepods, for example, can adjust their speed and direction of vertical migration by reorientation in response to hydrodynamic signals (Strickler & Bal 1973). Other organisms behave in similar ways. Veliger larvae are thought to respond to large fluid accelerations or strains (Fuchs *et al.* 2013) to avoid local turbulence (Barile, Stoner & Young 1994). Oyster larvae increase their upward swimming speed but also perform rapid dives when the intensity of turbulence increases (Fuchs *et al.* 2015). Rapid morphology changes allow dinoflagellates to diversify their direction of migration in intense turbulence, probably to enhance the chance of survival of the population. Sometimes these organisms form long chains to increase their swimming speeds (Fraga 1989; Sullivan *et al.* 2003) to increase their speed of vertical migration (Lovecchio *et al.* 2019).

How did these strategies evolve? This question requires answers on different levels. From an evolutionary perspective, what is the cost or reward function to be optimised? Is it more important to avoid predation or to find food in an efficient way? Organisms like copepods or larvae migrate upward to the water surface to feed (Hays 2003), but migrate downward during the day or in the presence of strong turbulence (Incze *et al.* 2001; Barile *et al.* 1994), to hide in darkness from foraging predators (Bollens & Frost 1989) or to avoid turbulence because it is easier to detect a predator in a quiescent fluid (Visser 2001; Gilbert & Buskey 2005).

To pursue these questions starting from a mechanistic model for a micro-swimmer in a complex flow poses several challenges, not least concerning the fluid mechanics of small swimming organisms. First of all, which signals can an active micro-organism measure, and how? This is quite well understood (Visser 2010). Plankton as small as tens of microns (Martens *et al.* 2015) can detect hydrodynamic signals in the form of fluid disturbances using sensory hairs such as setae or cilia. Planktonic copepods, for example, use arrays of setae to detect small velocity differences to the ambient flow. From the bending patterns of their setae, these organisms can also distinguish their relative angular velocity to the fluid, as well as its strain rate (Kiørboe, Saiz & Visser 1999). Ciliates (Jakobsen 2001) and rotifers (Kirk & Gilbert 1988) use similar mechanisms to detect predators. Also, invertebrate larvae can sense fluid strains by the deformation of cilia (Mackie, Singla & Thiriot-Quievreux 1976; Fuchs *et al.* 2015).

Second, given a reward function to optimise, which environmental signals are the most important? As mentioned above, fluid strains may indicate the presence of predators (Kiørboe & Visser 1999), but the fluid-velocity gradients caused by a predator may be masked by local turbulent fluctuations (Visser 2001; Gilbert & Buskey 2005). Moreover, a sinking organism may measure its settling velocity to infer the direction of gravity. This may allow the organism to reorient to navigate vertically (Strickler & Bal 1973). Finally, fluid-velocity fluctuations generated by flow around obstacles on the sea floor may indicate appropriate habitats for larval organisms (Fuchs *et al.* 2015).

Third, given certain environmental cues, what should the swimmer do? It should act rationally (Visser 2010), because the strategies evolved under natural selection must benefit the survival of the organism. Different species developed different strategies. Copepods tend to jump when they sense a fluid disturbance caused by a predator (Kiørboe *et al.* 1999) or they may adjust their cruising speeds in response to a changing turbulence intensity (Michalec, Souissi & Holzner 2015). Sometimes, a copepod may change not only

its swimming speed but also its swimming direction (Kiørboe *et al.* 2010). When oyster larvae sense a change in turbulent intensity close to the seafloor, they dive and attach to the floor (Fuchs *et al.* 2013). Phytoplankton can modulate the efficiency of vertical migration (Durham *et al.* 2013; Gustavsson *et al.* 2016) in response to turbulence, by changing their cellular morphology (Sengupta, Carrara & Stocker 2017) or forming cell chains (Park *et al.* 2001; Lovecchio *et al.* 2019).

Fourth, if one tracks a micro-organism in a complex or turbulent flow, how should one interpret its actions? The challenge is that the cues may change in an apparently random fashion as the organism explores the flow. In general, it is difficult to model the time sequence of environmental cues because it depends on the actions the swimmer chooses to take. In addition, what looks like a good move at any moment may turn out not to be optimal in the long run.

In summary, the question is how to find optimal strategies to optimise a given reward for a micro-swimmer in a complex flow and how to understand the mechanisms that determine the optimal strategy. In a recent proof-of-principle study, Colabrese *et al.* (2017) demonstrated that reinforcement learning is an efficient way to address this question. The authors used the Q-learning algorithm (Watkins & Dayan 1992; Sutton & Barto 1998; Mehlig 2021) to investigate strategies for efficient vertical migration of a gyrotactic micro-swimmer. The point is that fluid-velocity gradients tend to re-orient the swimmer, which make it difficult to find the optimal path to the surface. Colabrese *et al.* (2017) analysed different swimming strategies for an idealised model of a swimmer in a two-dimensional steady vortex flow. The swimmer measured the local vorticity of the flow, whether it was positive, negative or close to zero, and whether the current swimming direction pointed left, right, up or down in the laboratory frame. The possible actions were to swim left, right, up or down. Colabrese *et al.* (2017) demonstrated that smart swimmers can avoid being trapped in vortices and that they can take advantage of upwelling flows to accelerate upward navigation. This work motivated some follow-up studies (Gustavsson *et al.* 2017; Colabrese *et al.* 2018; Alageshan *et al.* 2020; Qiu *et al.* 2020), which investigated different flows as well as different actions. In all of these studies, some signals and actions referred to the laboratory frame, so that the swimmer had, in effect, access to a map, which facilitated navigation. The navigation problems considered in recent studies (Biferale *et al.* 2019; Schneider & Stark 2019; Gunnarson *et al.* 2021; Muiños-Landin *et al.* 2021) also used information relating to a fixed reference frame.

Motile micro-organisms in a complex flow, by contrast, do not carry a map. They can only access limited information regarding the local flow field. By detecting the velocity difference to the surrounding flow, a micro-swimmer can estimate the local fluid-velocity gradients or its rotation relative to that of the local fluid. In some cases, a swimmer might have access to global information. During day time, it can, for instance, follow the light to find the way to the surface (phototaxis) (Cohen & Forward 2002). This does not work at night or under conditions where it is hard to determine the light direction. The question is therefore how a micro-swimmer can successfully navigate a complex flow given that it has only local information in its frame of reference. The answer to this question depends on the reward function and, in particular, on its symmetries. We expect that a task that does not break any symmetry of the problem is easiest to learn, such as escaping from a certain point as far as possible in a given time with a given swimming speed. Efficient upward migration, by contrast, may be more difficult to learn because it requires that the problem does not have vertical reflection symmetry.

In this paper, we use reinforcement learning to find efficient strategies for vertical migration using only local signals and local actions. We use a highly idealised model

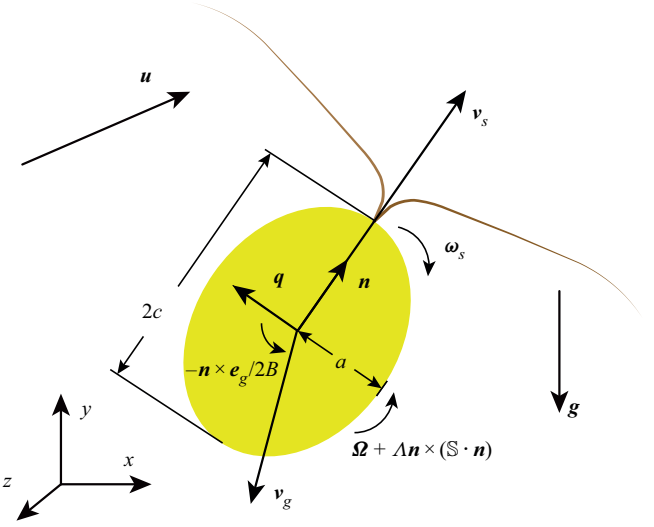

Figure 1. Sketch of an elongated micro-swimmer in the x–y plane, which shows the velocities and angular velocities that determine the dynamics of the micro-swimmer (see (2.1)).

for a motile micro-organism and its hydrodynamic sensing capabilities. With Q-learning, we search for optimal strategies for fast vertical migration in a two-dimensional steady Taylor–Green vortex flow (Taylor 1923), which allows for direct comparison with Colabrese *et al.* (2017), and in a steady two-dimensional random velocity field. We investigate how symmetry breaking allows the swimmer to distinguish different directions (which is necessary to swim upwards), which highlights significant differences between navigation using local signals in the frame of reference of the swimmer and signals in the laboratory frame (Colabrese *et al.* 2017, 2018; Gustavsson *et al.* 2017; Biferale *et al.* 2019; Schneider & Stark 2019; Alageshan *et al.* 2020; Gunnarson *et al.* 2021; Muiños-Landin *et al.* 2021). We find that settling owing to gravity allows the swimmers to find efficient strategies for vertical migration, because the settling breaks vertical reflection symmetry. We show that the swimmers emulate more slender ones through adaptive steering, which enables them to preferentially sample upwelling regions of the flow and thus accelerate upward migration.

2. Methods

2.1. *Model*

Swimming gaits and speeds of motile micro-organisms vary substantially (Jiang, Osborn & Meneveau 2002; Fuchs & Gerbi 2016). Here we do not refer to any particular plankton species or to any particular mode of propulsion. Instead, we assume that the micro-swimmer cruises with a constant translational speed v_s (Durham, Kessler & Stocker 2009; Durham *et al.* 2013; Gustavsson *et al.* 2016; Lovecchio *et al.* 2019). Our idealised micro-swimmer can choose to rotate with angular velocity $\boldsymbol{\omega}_s$. We model the swimmer as an elongated spheroid with aspect ratio $\lambda = c/a$ and symmetry axis $\boldsymbol{n}$ (figure 1). In § 4, we discuss potential limitations of this highly idealised model.

For our analysis, we use model parameters typical for copepods in the ocean (table 1). Given the parameters in table 1, we infer that the Reynolds number $\mathrm{Re}_p = 2cv_s/\nu$ and the Stokes number $St = \tau_p/\tau_f$ are both small. Here, ν is the kinematic viscosity, τ_p is the

		Range	Value used	Unit
Swimmer size	$2c$	0.1–0.5	0.2	mm
Aspect ratio	2.0–2.5	2.0		
Mass–density ratio	ρ_p/ρ_f	1.005–1.019	1.017	
Swimming velocity	v_s	0.33–3.76	1.00	mm s^{-1}
Settling velocity	$v_g^{\parallel}$	0.1–0.8	0.152	mm s^{-1}
	$v_g^{\perp}$		0.133	mm s^{-1}
Swimming angular velocity	ω_s	<20.0	1.0	rad s^{-1}
Gyrotactic timescale	B	≈5.0	5.0	s

Table 1. Summary of model parameters. The swimmer size is obtained from the length of a small copepod (Titelman 2001; Titelman & Kiørboe 2003) and the aspect ratio is a rough estimate between the length and width of copepods (Carlotti, Bonnet & Halsband-Lenk 2007). The mass–density ratio is calculated using mass density of copepods ρ_p (Knutsen, Melle & Calise 2001) and a sea-water density of $\rho_f = 1.025$ g cm^{-3} (salinity of 3.5 % and temperature of 20 °C) (Millero *et al.* 1980). The value of the swimming velocity is typical of the values observed in experiments (Titelman & Kiørboe 2003). The settling velocity is estimated by Stokes settling velocity (Kim & Karrila 1991), which is consistent with the range given by Titelman & Kiørboe (2003). The maximal angular velocity can be estimated from the images shown by Jiang & Paffenhöfer (2004) to approximately 90° in 0.067 s. We use a lower value for convenience in numerical simulation, which represents the slow steering motion (Kabata & Hewitt 1971). The gyrotactic re-orientation time is taken from Fields & Yen (1997) for copepods.

particle response time for spheroids (Kim & Karrila 1991; Zhao *et al.* 2015) and τ_f is a characteristic flow time-scale (discussed in more detail below). Assuming that $\mathrm{Re_p} \ll 1$ and $St \ll 1$, we neglect the inertia of swimmer and fluid, and use the following overdamped model (Durham *et al.* 2013; Gustavsson *et al.* 2016) for the dynamics:

$$\dot{\boldsymbol{x}} = \boldsymbol{v}, \tag{2.1a}$$

$$\boldsymbol{v} = \boldsymbol{u} + v_s\boldsymbol{n} + \boldsymbol{v}_g + \boldsymbol{\xi}, \tag{2.1b}$$

$$\dot{\boldsymbol{n}} = \boldsymbol{\omega} \times \boldsymbol{n}, \tag{2.1c}$$

$$\boldsymbol{\omega} = \boldsymbol{\Omega} + \Lambda\boldsymbol{n} \times (\mathbb{S}\boldsymbol{n}) + \boldsymbol{\omega}_s - \frac{1}{2B}\boldsymbol{n} \times \boldsymbol{e}_g + \boldsymbol{\eta}. \tag{2.1d}$$

Here, $\boldsymbol{v}$ and $\boldsymbol{\omega}$ denote the velocity and the angular velocity of the swimmer, respectively. The first three terms on the right-hand side of (2.1*b*) denote the fluid velocity $\boldsymbol{u}(\boldsymbol{x}, t)$ at the swimmer position $\boldsymbol{x}$, the constant translational swimming speed v_s in the direction of $\boldsymbol{n}$ and the Stokes settling velocity $\boldsymbol{v}_g$ for a spheroid (Kim & Karrila 1991):

$$\boldsymbol{v}_g = v_g^{\perp}\boldsymbol{e}_g + [v_g^{\parallel} - v_g^{\perp}](\boldsymbol{e}_g \cdot \boldsymbol{n})\boldsymbol{n}. \tag{2.1e}$$

Here, $\boldsymbol{e}_g$ is the unit vector in the direction of gravity, and $v_g^{\parallel}$ and $v_g^{\perp}$ are the settling speed of a spheroid in a quiescent fluid aligned parallel with or perpendicular to gravity, respectively (Kim & Karrila 1991). The buoyancy of micro-swimmers varies depending on their living environment (Cohen *et al.* 2019). Here we assume that the mass density of the swimmer is larger than that of water (table 1).

The first two terms on the right-hand side of (2.1*d*) correspond to Jeffery's angular velocity for a spheroid, using the Stokes approximation (Jeffery 1922). These contributions

to the angular velocity depend on the flow vorticity $2\boldsymbol{\Omega}$, the strain $\mathbb{S}$ and the shape factor

$$\Lambda = \frac{\lambda^2 - 1}{\lambda^2 + 1}. \tag{2.2}$$

The third term on the right-hand side of (2.1*d*) represents the angular velocity owing to active rotations, $\boldsymbol{\omega}_s$. The fourth term is the gyrotactic angular velocity arising from a restoring torque towards $-\boldsymbol{e}_g$, with a time scale B (Kessler 1985; Visser 2010; Durham *et al.* 2013; Gustavsson *et al.* 2016). Finally, $\boldsymbol{\xi}$ and $\boldsymbol{\eta}$ in (2.1) represent small white-noise perturbations, added to remove the influence of initial position and orientation of the swimmers and to break structurally unstable periodic orbits (Colabrese *et al.* 2017).

In the present study, we consider only two-dimensional flows. Although (2.1) are compatible with three-dimensional motion, we restrict the translational and rotational motion of the swimmer to the x–y plane. We use two different models for the fluid-velocity field. First, to compare with Colabrese *et al.* (2017), we consider a two-dimensional, time-independent Taylor–Green vortex (TGV) flow with velocity (Taylor 1923):

$$\boldsymbol{u}(\boldsymbol{x}) = \boldsymbol{\nabla} \times \boldsymbol{e}_z \psi(\boldsymbol{x}) \text{ with stream function } \psi(\boldsymbol{x}) = -\frac{u_0 L_0}{2} \cos\frac{x}{L_0} \cos\frac{y}{L_0}. \tag{2.3}$$

Here $\boldsymbol{e}_z$ is the unit vector in the z-direction and we assume that the gravitational acceleration points in the negative y-direction, $\boldsymbol{e}_g = -\boldsymbol{e}_y$, as shown in figure 1. We take $u_0 = 2.0$ mm s^{-1} and $L_0 = 0.5$ mm for the velocity and length scales of the flow, and define $\tau_f \equiv L_0/u_0$. These scales correspond to the Kolmogorov scales (Frisch 1997) of ocean turbulence with kinematic viscosity $\nu \sim 10^{-6}$ m^2 s^{-1} and energy dissipation rate $\mathcal{E} = 1.6 \times 10^{-5}$ m^2 s^{-3} (Yamazaki & Squires 1996). Following the values in table 1 and the assumed velocity and length scales of the flow, the non-dimensional parameters of swimming velocity and gyrotactic stability (Durham, Climent & Stocker 2011; Colabrese *et al.* 2017) are

$$\Phi \equiv \frac{v_s}{u_0} = 0.5 \quad \text{and} \quad \Psi \equiv \frac{BL_0}{u_0} = 20. \tag{2.4a,b}$$

Comparing with Durham *et al.* (2011) and Colabrese *et al.* (2017), who explored a parameter range of $0.01 < \Phi, \Psi < 100$, our swimmers have low swimming speeds and weak gyrotaxis. Therefore, they cannot migrate efficiently unless they actively adjust their swimming directions.

To verify the generality of the results obtained for the TGV flow, we compare with the results obtained using a Gaussian random velocity field. This velocity field is defined by a stream function $\psi(\boldsymbol{x})$ with zero mean and correlation function (see Gustavsson & Mehlig (2016) for details)

$$\langle \psi(\boldsymbol{x}) \psi(\boldsymbol{x}') \rangle = \frac{\ell^2 u_{s,0}^2}{2} \exp\left[-\frac{|\boldsymbol{x} - \boldsymbol{x}'|^2}{2\ell^2} \right]. \tag{2.5}$$

We choose the parameters ℓ and $u_{s,0}$ so that the spatial averages of $\boldsymbol{u}^2$ and $\sum_{i,j} (\partial_i u_j)^2$ are equal those obtained from (2.3).

2.2. *Hydrodynamic signals*

Many planktonic micro-swimmers can sense the motion of the surrounding fluid using sensory hairs which allow to detect velocity differences between the body and the fluid

(Mackie *et al.* 1976; Kirk & Gilbert 1988; Kiørboe & Visser 1999; Jakobsen 2001; Visser 2010; Fuchs *et al.* 2013). For example, to a first approximation, a micro-swimmer can be considered rigid so that it cannot deform. If the surrounding fluid deforms with strain rate $\mathbb{S}$, velocity differences $\boldsymbol{\delta}_s$ must arise between the surface velocity of the swimmer and the fluid velocity: $\boldsymbol{\delta}_s = \mathbb{S}\boldsymbol{r}$, where $\boldsymbol{r}$ is the vector from the centre of the swimmer to a point on its surface (Kiørboe & Visser 1999). In this way, a swimmer can detect the fluid strain rate in its local frame of reference. This argument neglects the fact that the swimmer disturbs the flow. Strictly speaking, it can therefore not directly measure the undisturbed fluid strain while swimming. Accurate measurement of the strain rate is difficult when the swimming speed is of the same order of magnitude as the fluid velocity (Visser 2010). However, it is thought that organisms can distinguish external fluid-velocity disturbances from those generated by their own motion (Yen & Strickler 1996). For example, copepods can sense external hydrodynamic signals while they generate their own feeding current (Hwang & Strickler 2001). Also, steady swimming generates definite fluid-velocity gradients around the swimmer which makes it possible, in principle, to subtract these gradients from an external signal.

At any rate, for an incompressible velocity field in two dimensions, there are two independent strain parameters. Assuming that the swimmer can measure the normal and tangential components of the fluid strain rate tensor along its swimming direction, we take the independent components to be

$$S_{nn} = \boldsymbol{n} \cdot \mathbb{S}\boldsymbol{n}, \tag{2.6a}$$

$$S_{nq} = \boldsymbol{n} \cdot \mathbb{S}\boldsymbol{q}. \tag{2.6b}$$

Here $\boldsymbol{n}$ is the swimming direction defined above and $\boldsymbol{q}$ is a vector orthogonal to $\boldsymbol{n}$, such that $\boldsymbol{n}$ and $\boldsymbol{q}$ form a right-handed orthonormal basis in the flow plane (figure 1).

Relative rotation between the fluid and the swimmer also results in velocity differences on the surface of the swimmer, given by $\boldsymbol{\delta}_\Omega \sim (\boldsymbol{\Omega} - \boldsymbol{\omega}) \times \boldsymbol{r}$, where both $\boldsymbol{\Omega}$ and $\boldsymbol{\omega}$ are parallel to $\boldsymbol{e}_z$ in a two-dimensional flow. Relative angular motion results from the gyrotactic torque (Visser 2010) or simply because the swimmer rotates actively. We assume that the swimmer can measure local relative rotation:

$$\Delta\Omega = (\boldsymbol{\Omega} - \boldsymbol{\omega}) \cdot \boldsymbol{e}_z. \tag{2.6c}$$

Finally, a swimmer can also measure the local slip velocity owing fluid acceleration, swimming or settling (Visser 2010). In two spatial dimensions, there are two independent components of the slip velocity:

$$\Delta u_n = (\boldsymbol{u} - \boldsymbol{v}) \cdot \boldsymbol{n}, \tag{2.6d}$$

$$\Delta u_q = (\boldsymbol{u} - \boldsymbol{v}) \cdot \boldsymbol{q}. \tag{2.6e}$$

To implement the Q-learning algorithm, we must discretise the signals. Appropriate discretisation scales can be estimated from the threshold of sensing velocity differences Δu_c and from the size c of the swimmer (Kiørboe & Visser 1999). This results in the following scales for the thresholds of strain $S_c = \Delta u_c/c$ and angular slip velocity $\Delta\Omega_c = \Delta u_c/c$. Thresholds estimated using the half-length of the major axis c (instead of the minor axis a) reflect the highest sensitivity to signals for spheroidal swimmers: any signal below these thresholds cannot give rise to a velocity difference greater than Δu_c anywhere on the swimmer surface. In experiments, it is observed that copepods make escape jumps in response to strain rates with threshold values in a range of more than one order of magnitude (Kiørboe *et al.* 1999; Buskey *et al.* 2002). Here we adopt a typical

Signal		Threshold	
Strain rate	S_{nn}, S_{nq}	$S_c = 0.5$	s^{-1}
Angular slip velocity	$\Delta\Omega$	$\Delta\Omega_c = 0.5$	s^{-1}
Slip velocity	Δu_q	$\Delta u_c = 50$	$\mu\mathrm{m\ s}^{-1}$

Table 2. Summary of signals and thresholds we use in Q-learning. The threshold values S_c, $\Delta\Omega_c$ and Δu_c are used to discretise the signals for Q-learning. The value of S_c is taken from experiments where copepods are observed to jump in response to strain rates above $\sim$0.5 s^{-1} (Kiørboe *et al.* 1999; Buskey, Lenz & Hartline 2002). The values of $\Delta\Omega_c$ and Δu_c are then estimated from S_c, see text.

value, $S_c \sim 0.5\ \mathrm{s}^{-1}$, corresponding to $\Delta u_c = cS_c \sim 50\ \mu\mathrm{m\ s}^{-1}$, which is of the same order of magnitude as the smallest velocity difference, 20 $\mu\mathrm{m\ s}^{-1}$, that a copepod can measure (Yen *et al.* 1992). From this value, we also obtain $\Delta\Omega_c = S_c = 0.5\ \mathrm{s}^{-1}$ from the definition above. The signal Δu_n, evaluated using the swimming speed in table 1, lies below the lower threshold, $\Delta u_n < -\Delta u_c$. This signal is therefore always activated and the swimmer can therefore not distinguish changes of the signal Δu_n close to the threshold value. Rather than introducing new, arbitrary thresholds for Δu_n, we focus on the other four signals in (2.6) in what follows, on S_{nn}, S_{nq}, $\Delta\Omega$ and Δu_q. In table 2, we summarise the signals and thresholds used.

2.3. *States and actions*

To apply the Q-learning algorithm in its simplest form, we must define states and actions. The state of the swimmer is obtained from local measurements of the environment. Given the thresholds quoted above, we discretise each of the signals in table 2 into three states. For example, the possible values of S_{nn} are discretised into three intervals $S_{nn} < -S_c$, $-S_c < S_{nn} < S_c$ and $S_{nn} > S_c$.

Depending on the state of swimmer, it may take different actions. In our model, the swimmer moves with constant speed while steering with an angular velocity $\boldsymbol{\omega}_s$ (Kabata & Hewitt 1971). For two-dimensional flows, only the z-component, $\omega_s \equiv \boldsymbol{\omega}_s \cdot \boldsymbol{e}_z$, matters. We allow the swimmer to choose between three values of ω_s,

$$\omega_s = \{-1, 0, 1\}\ \mathrm{rad\ s}^{-1}, \tag{2.7}$$

to control its motion. In other words, the swimmer either swims straight ahead, $\omega_s = 0$, or steers with a constant positive or negative angular velocity.

More choices of steering actions might enhance the reward of the optimal strategy. However, here we only consider the three possibilities (2.7), because a larger number of actions may lead to strategies that are less robust because of overfitting. Also, a larger number of actions will result in a great difficulty to find candidates for optimal strategies. Fewer actions tend to result in strategies that we can interpret and understand. We choose 1 rad s^{-1} for the magnitude of the steering angular velocity, which is one quarter of the maximum flow vorticity, because this allows the swimmer to exert some orientational control in regions of lower vorticity. This value is smaller, by a factor of ten, than the angular velocity that would be obtained if the swimmer were to convert its full propulsion effort into angular motion, $\omega_{max} \sim v_s/c \sim 10\ \mathrm{rad\ s}^{-1}$. This means that the steering motion only requires a small amount of energy compared with that required for propulsion. We also remark that some micro-swimmers can achieve much higher angular velocities,

up to approximately 20 rad s^{-1}, when they rotate rapidly (Jiang & Paffenhöfer 2004). Our model does not describe such vigorous motion.

These states and actions are local. They refer to the frame of reference of the swimmer and do not directly relate to the laboratory frame. We contrast this with the states and actions stipulated by Colabrese *et al.* (2017). They defined the states of the swimmer in terms of discrete orientations in the laboratory frame (left, right, up or down), and the three discretised levels of the vorticity of background flow [$\Omega_z < -\Omega_c$, $-\Omega_c < \Omega_z < \Omega_c$ and $\Omega_z > \Omega_c$, with the threshold $\Omega_c = u_0/(6L_0)$]. The actions of the swimmer in Colabrese *et al.* (2017) were to rotate with angular velocity

$$\boldsymbol{\omega}_s = \frac{1}{2B}(\boldsymbol{n} \times \boldsymbol{k}). \tag{2.8}$$

The vector $\boldsymbol{k}$ is chosen by the swimmer from four possible directions (left, right, up or down) in the laboratory frame in the x–y plane. Below we compare strategies obtained for both models.

2.4. *Q-learning*

The task of the swimmer is to navigate upward through the flow. As mentioned in § 1, vertical migration is common and important for micro-organisms in the ocean. Because this task breaks vertical reflection symmetry, it allows us to illustrate the role of symmetries in the learning problem. To find optimal upward navigation strategies, we use the reward function

$$r_i = \frac{1}{L_0}(y_{i+1} - y_i). \tag{2.9}$$

Here y_i is the vertical location of the swimmer immediately after a state update $s_{i-1} \to s_i$. For the simulation in TGV flow, states are updated at a fixed time-step size and the reward r_i is thus proportional to the time-averaged velocity from s_i to s_{i+1}. This allows the algorithm to optimise the vertical navigation velocity. For the simulation in random velocity fields, states are updated only when one of the state signals changes its discretised state level, and r_i is only approximately proportional to a velocity (see Appendix A). We have confirmed that these two update rules give the same result in TGV flow.

We use the one-step Q-learning algorithm (Watkins & Dayan 1992; Sutton & Barto 1998; Mehlig 2021) to search for efficient strategies for vertical migration. The swimmers move according to the dynamics (2.1) with ω_s adjusted according to the current state. When evaluating strategies, we use a greedy choice of action: whenever the state is updated to s_i, the swimmer takes the action $a_i = \arg\max_a Q(s_i, a)$. The value function $Q(s_i, a)$ is an estimate of the summation of future reward if action a is taken at state s_i, also referred to as the Q table. To find an estimate of the Q table, we use a training phase, where the swimmer adopts the ε-greedy strategy: it mainly takes the action $a_i = \arg\max_a Q(s_i, a)$ but takes a random action with a probability ε. This allows the swimmer to explore different actions and helps to avoid local optima. Given $\{s_i, a_i, r_i, s_{i+1}\}$, the Q table is updated in the standard fashion during the training phase:

$$Q(s_i, a_i) \leftarrow Q(s_i, a_i) + \alpha\left[r_i + \gamma \max_a Q(s_{i+1}, a) - Q(s_i, a_i)\right]. \tag{2.10}$$

The learning rate α is a free parameter that controls the convergence speed. The rate γ, $0 \le \gamma < 1$, is introduced to regularise the discounted reward $\sum_{j=i}^{\infty} r_j \gamma^{j-i}$. We choose $\gamma = 0.999$ to obtain a far-sighted strategy. The training is divided into episodes. In each

Case	State	Action	Settling	Gyrotaxis	Vertical reflection symmetry	Training
S1	S_{nq}, S_{nn}	(2.7)	No	No	Unbroken	Failure
S2	$\Omega_z, \boldsymbol{n}$	(2.7)	No	No	Broken ($\boldsymbol{n}$ known in lab frame)	Success
S3	S_{nq}, S_{nn}	(2.8)	No	No	($\boldsymbol{k}$ known in lab frame)	Success
S4	S_{nq}, S_{nn}	(2.7)	No	Yes	Broken (gyrotaxis)	Success
S5	S_{nq}, S_{nn}	(2.7)	Yes	No	Broken (settling)	Success
S6	S_{nq}, S_{nn}	(2.7)	Yes	Yes	Broken (gyrotaxis and settling)	Success

Table 3. Summary of cases studied (see text for definitions of $\boldsymbol{n}$ and $\boldsymbol{k}$, and further details).

episode, ten swimmers sharing the same Q table are initialised with random locations and orientations. Each episode allows for at least $i_{max} = 10^4$ state changes, large enough for the discounted reward to converge. We choose the number of episodes large enough for the Q table to converge to an approximately optimal policy. The training details are slightly different for the TGV flow and for the random velocity fields. Further details concerning the training and parameter values are given in Appendix A.

2.5. *Summary of cases studied*

As mentioned in § 1, our goal is to investigate the role of symmetries in finding optimal strategies for vertical migration. Table 3 summarises the different cases we analyse, S1–S6. The TGV flow has C_4 point-group symmetry, and the random velocity field is statistically isotropic (its correlation functions are isotropic). As a consequence, both velocity fields exhibit vertical reflection symmetry. The swimmer cannot distinguish the $\boldsymbol{e}_y$-direction – it cannot find any meaningful strategy for vertical navigation – unless the vertical reflection symmetry of the problem is broken. In case S1, both states and actions are local, and neither settling nor gyrotaxis are taken into account. Hence, neither signals, nor actions nor the dynamics break vertical reflection symmetry. Therefore, the swimmer fails to find a strategy to move in the $\boldsymbol{e}_y$-direction. In the cases S2 and S3, vertical reflection symmetry is broken because the swimmer either knows its orientation in the lab frame (it knows whether $\boldsymbol{n}$ points up or down, case S2) or it has an absolute sense of the target direction ($\boldsymbol{k}$ in (2.8), case S3). These two cases are similar to those studied by Colabrese *et al.* (2017). Because the swimmer has direct access to the laboratory coordinates, it learns to navigate as expected. For cases S4 and S5, neither states nor actions break the vertical reflection symmetry. In this case, the swimmer can learn to migrate along the $\boldsymbol{e}_y$-direction if its dynamics breaks the symmetry, either because the swimmer experiences a gyrotactic torque or because it is heavier than the fluid and settles along the negative $\boldsymbol{e}_y$-direction. These cases are analysed in § 3.1.

It is clear that gyrotaxis in case S4 must help the swimmer to navigate successfully, because it tends to align $\boldsymbol{n}$ with the $\boldsymbol{e}_y$-direction. However, training can be successful even in the absence of gyrotaxis. It might appear that settling alone should make it more difficult for the swimmer in case S5 to navigate upwards, because settling imposes a negative contribution to v_y after all. However, in the absence of any other symmetry breaking, settling may enable the swimmer to move upwards although gravity pulls it down.

Finally for case S6, both settling and gyrotaxis act with the parameters given in table 1. This case is analysed in § 3.2 to understand the microscopic mechanisms that allow the swimmer to navigate with local signals and actions.

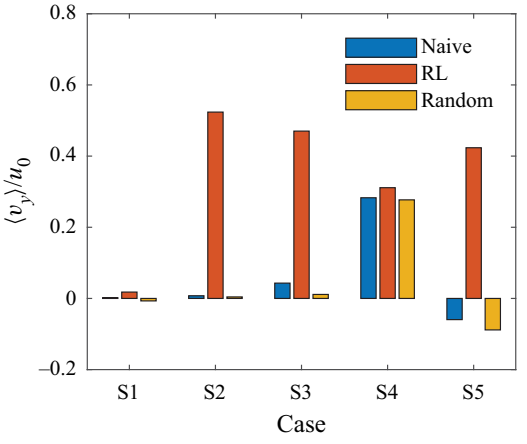

Figure 2. Normalised averaged vertical velocity $\langle v_y \rangle$ for cases S1–S5 (table 1). Shown are the results following the naive strategy ('naive', see text), the best strategy obtained by reinforcement learning ('RL') using the signals S_{nn} and S_{nq}, and a random strategy ('random'), where the swimmer takes random actions when its state, defined by S_{nn} and S_{nq}, changes.

3. Results

3.1. *Symmetry breaking*

To find the optimal strategy with reinforcement learning, we use a subset of signals, only S_{nn} and S_{nq}. Each signal gives rise to three states so that the size of the Q table is $3^2 \times 3$, which corresponds to nine states and three actions. Thus, a swimmer can choose between $3^9 \sim 10^4$ different strategies in total. In principle, one can evaluate the performance of each possible strategy, but Q-learning allows us to obtain optimal or approximately optimal strategies much more efficiently. Figure 2 illustrates the training results for cases S1–S5 (table 3). Shown is the average velocity of the swimmer $\langle v_y \rangle$ (see (2.1*b*)) in the y-direction, after the velocity reaches a statistically steady state. Angular brackets represent the ensemble average over the positions of swimmers. Red bars show the results of the best strategy obtained after training in each case.

To assess the success of the optimal strategy, we compare it with two others. First, we consider a swimmer that follows the 'naive' strategy, which follows a single predefined action. For S3, this means that ω_s is chosen according to (2.8) with $\boldsymbol{k} = \boldsymbol{e}_y$, so that the swimmer always turns towards the $\boldsymbol{e}_y$-direction in the laboratory frame (Colabrese *et al.* 2017). This strategy breaks the vertical reflection symmetry. For cases S2, S4 and S5, the naive strategy corresponds to $\omega_s = 0$, which does not break this symmetry. Second, adopting a random strategy, the swimmer chooses a random action with equal probability whenever the state defined by S_{nn} and S_{nq} changes. The random strategy preserves the point-group symmetry, at least on average.

Figure 2 shows, as expected, that training fails in the completely symmetric case S1. The results for cases S2 and S3 confirm, as expected, that the swimmers find strategies to optimise vertical migration when either signals or actions break the symmetry of the flow (Colabrese *et al.* 2017). We also see that the optimal strategy found by reinforcement learning is better than both naive or random strategies, which resultsin a larger $\langle v_y \rangle$. Cases S4 and S5 show that the swimmer can still learn to optimise vertical migration. In both cases, the vertical reflection symmetry is neither broken by signals nor actions, but by the dynamics. With gyrotaxis alone (no settling, case S4), the optimal strategy is only

slightly better than the naive one. This is not surprising because the naive strategy breaks the symmetry. It is interesting, however, that settling alone helps the swimmer to navigate upwards (no gyrotaxis, case S5). If the symmetry is not broken in any other way, settling is in fact necessary to allow the swimmer to find the positive $\boldsymbol{e}_y$-direction. We see in figure 2 that the signals S_{nn} and S_{nq} provide enough information for the swimmer to actively exploit the flow. In the next section, we discuss the underlying mechanisms.

3.2. *Mechanisms*

How does the swimmer make use of local signals to navigate? We consider a swimmer following the dynamics (2.1), with the parameters given in table 1. The steering angular velocities are $\omega_s = -1, 0, 1$ rad s^{-1} as described in § 2.3, and the signals are taken to be subsets of those listed in table 2. Figure 3 refers to four different combinations: S_{nq} alone; S_{nn} and S_{nq}; Δu_q and S_{nq}; $\Delta\Omega$ and S_{nq}. The key message is that S_{nq} alone allows the swimmer to successfully navigate. The corresponding Q table is shown in figure 3(*a*) and typical trajectories of swimmers following this strategy are shown in panel (*b*). We see that the swimmer learns to avoid the regions of strong vorticity and finds upwelling regions where the background flow tends to carry it upwards. Figure 4 illustrates that this behaviour is not particular to the TGV flow. Panel (*a*) shows how smart swimmers preferentially sample the upwelling fringes of the vortices in the TGV flow: they swim to the right of positive vortices (with $\Omega > 0$, white) and to the left of negative vortices (black). Panel (*b*) shows the same but for swimmers navigating a spatially smooth, steady random velocity field (see (2.5)). This suggests that the learnt strategy is robust, at least for steady two-dimensional flows, for parameter values similar to those shown in table 1.

The underlying strategy in figure 3(*a*) relies entirely on the signal S_{nq}. For a swimmer moving in a two-dimensional plane (the x–y-plane), we have

$$S_{nq} = \boldsymbol{n} \cdot \mathbb{S}\boldsymbol{q} \ = \boldsymbol{e}_z \cdot [\boldsymbol{n} \times (\mathbb{S}\boldsymbol{n})]. \tag{3.1}$$

Comparing with the equation of motion (see (2.1*d*)), we see that S_{nq} determines how the strain rotates the swimmer. When S_{nq} is negative, for example, a prolate swimmer ($\Lambda > 0$) is rotated clockwise by the strain. Figure 3(*a*) and (*b*) show that the optimal action does the same: $\omega_s < 0$ means that the swimmer steers clockwise. For $S_{nq} > 0$, however, the flow turns the swimmer counter-clockwise and so does the optimal action. Finally, when S_{nq} is close to zero, the swimmer does not actively steer.

Because the steering mirrors the effect of the strain, we conclude that the swimmer tries to emulate a more slender swimmer, with a larger value of Λ. This makes sense, because it was shown by Gustavsson *et al.* (2016) that naive gyrotactic swimmers (no steering actions, $\omega_s = 0$) tend to sample upwelling regions of the flow when their shape factor Λ increases, or at least regions where downwelling is weaker. In other words, the smart swimmers manage to preferentially sample upwelling regions of the flow by mimicking slender naive swimmers that take no steering actions ($\omega_s = 0$). How this works is shown more quantitatively in figure 5, where we compare the performance of smart swimmers with $\Lambda = 0.6$ to naive gyrotactic swimmers with $\Lambda \geq 0.6$. Figure 5 shows their mean vertical velocities $\langle v_y \rangle$, and also the different contributions to $\langle v_y \rangle$, namely $\langle n_y \rangle v_s$, $\langle u_y \rangle$ and the average vertical component of the settling velocity, $\langle \boldsymbol{v}_g \cdot \boldsymbol{e}_y \rangle$. We see that the smart swimmers have an appreciable upward velocity, because gyrotaxis favours alignment between $\boldsymbol{n}$ and $\boldsymbol{e}_y$, and because the swimmers sample upwelling regions where $u_y > 0$. Naive swimmers with the same value of Λ also migrate upwards, but more slowly. Figure 5 reveals the reason: naive swimmers do not sample upwelling regions as efficiently as smart

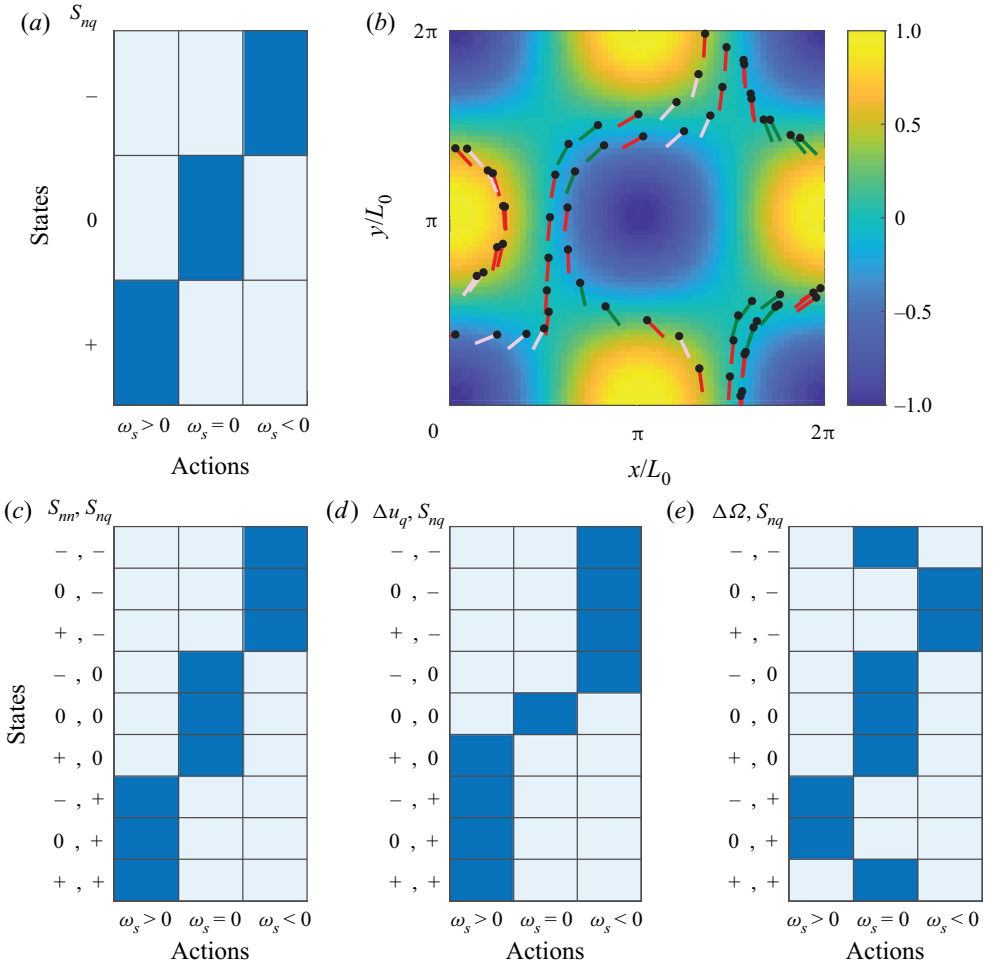

Figure 3. (*a*) Q table of the optimal strategy when swimmers sense only S_{nq}. Each signal has three levels: negative (−), approximately zero (0) or positive (+), as described in § 2.3. The cells filled with blue indicate the optimal action for each state. (*b*) Typical trajectories of smart swimmers following the strategy shown in panel (*a*). Black dots represent the instantaneous position of the swimmer and the coloured line segments indicate the swimmer orientation $\boldsymbol{n}$ (representing the tail of the swimmer). The colours represent signals and corresponding actions: green, $S_{nq} < 0$, $\omega_s < 0$; red, $S_{nq} \approx 0$, $\omega_s = 0$; salmon, $S_{nq} > 0$, $\omega_s > 0$. The background colour gives the normalised vorticity $2\Omega_z L_0/u_0$. Remaining panels: Q tables for different signal choices, using (*c*) S_{nn} and S_{nq}; (*d*) Δu_q and S_{nq} and (*e*) $\Delta\Omega$ and S_{nq}.

ones and do not align as much with the upward direction. Figure 5 also illustrates that naive swimmers with larger values of Λ tend to sample upwelling regions more efficiently ($\langle u_y \rangle$ is larger) and align more with the upward direction than in the case $\Lambda = 0.6$. For a spheroid, the shape factor Λ is constrained to be smaller than unity (see (2.2)). It is nevertheless interesting to investigate the dynamics for larger values of Λ, artificially increasing the effect of the strain on the angular dynamics (Zhao *et al.* 2019). Here, we change the value of Λ, but keep λ, $v_g^{\parallel}$ and $v_g^{\perp}$ constant, as given in table 1 (this means that (2.2) no longer holds).

Figure 5 shows that a smart swimmer with shape factor $\Lambda = 0.6$ migrates as fast as a naive swimmer with $\Lambda = 1.2$, roughly twice as fast as a naive swimmer of the

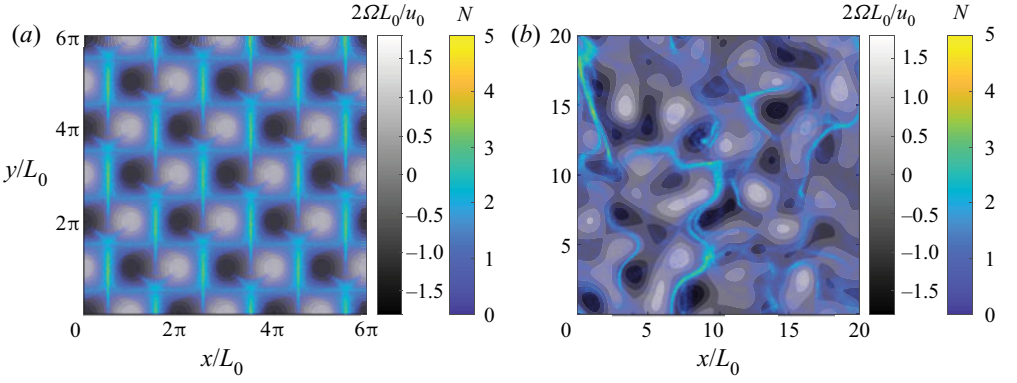

Figure 4. Number density N of swimmers following the dynamics (2.1) with angular swimming ω_s according to the strategy in figure 3(a) (colour scale) in (a) the TGV flow (2.3) and (b) the random velocity field (2.5). The grey background scale refers to the normalised fluid vorticity, $2\Omega L_0/u_0$.

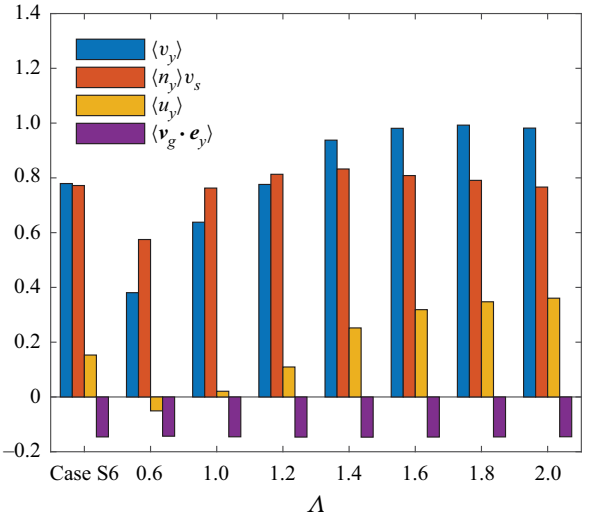

Figure 5. Contributions to the vertical swimming of swimmers defined in case S6 (the leftmost group) and naive swimmers with different Λ (the other groups) in the TGV flow. The blue bars represent the average of vertical velocity $\langle v_y \rangle$. The red, yellow and purple bars represent the vertical velocity owing to swimming, advection of local fluid and settling, respectively. All velocities are normalised by the swimming velocity v_s.

same parameter $\Lambda = 0.6$. We see that the average vertical velocity $\langle v_y \rangle$ increases as Λ grows until $\Lambda = 2$. This is explained by three observations. First, the average vertical swimming velocity $\langle n_y \rangle v_s$ increases as Λ increases from 0.6 to 1.4, because $\boldsymbol{n}$ tends to align with $\boldsymbol{e}_y$. However, note that the alignment becomes weaker for $\Lambda > 1.4$. Second, as predicted by Gustavsson *et al.* (2016) and later verified by direct numerical simulations of turbulence (Borgnino *et al.* 2018; Cencini *et al.* 2019; Lovecchio *et al.* 2019), the dynamics of gyrotactic swimmers undergoes a flow-and-parameter dependent transition from preferential sampling of downwelling regions for $\Lambda < \Lambda_c$ to upwelling regions for $\Lambda > \Lambda_c$. For the TGV flow and parameters leading to figure 5, this transition occurs at $\Lambda_c \approx 1$, as shown in figure 5. This implies that naive gyrotactic swimmers cannot sample upwelling regions. Smart swimmers, however, succeed in sampling upwelling regions by

emulating naive swimmers with $\Lambda > 1$. Third, the settling velocity $\langle \boldsymbol{v}_g \cdot \boldsymbol{e}_y \rangle$ is found to be almost independent of Λ. This is explained by the observation that the orientation $\boldsymbol{n}$ has only a small influence on the settling velocity because $v_g^{\parallel}$ and $v_g^{\perp}$ are of the same order of magnitude for the parameters given in table 1. These three observations explain the strategy shown in figure 3(*a*), as well as the trajectory patterns shown in figures 3(*b*) and 4.

Up to now, we discussed the simplest case, where the swimmers sense only one signal, S_{nq} (figure 3(*a*)). Now consider the cases where the swimmers sense not only S_{nq} but also other signals. In each case, we obtain an efficient strategy as shown in figure 3(*c–e*). These strategies are robust, because they are learnt in both TGV flow and a random velocity field. However, these strategies are only slightly better than the one in figure 3(*a*): the resulting upward velocities are of the same order of magnitude for all the four strategies (figure 7). Moreover, these strategies share a similar pattern. For instance, the strategy in figure 3(*c*) yields actions independent of the signal S_{nn}. In other words, it is identical to the strategy obtained using only S_{nq} as a signal (figure 3(*a*)). For the cases where the swimmers measure Δu_q or $\Delta\Omega$ in addition to S_{nq}, the Q tables shown in panels (*d*) and (*e*) illustrate that Δu_q is useful only when S_{nq} is close to zero, and $\Delta\Omega$ is useful only when S_{nq} and $\Delta\Omega$ are either both positive or negative. This means measuring extra signals in addition to S_{nq} provides not much more useful information for the upward navigation of swimmers. We therefore conclude that it is S_{nq} that provides the most important information, because in two-dimensional flows, it is a direct measure of the rotation the fluid strain exerts upon the swimmer and it allows the swimmers to smartly mimic more elongated swimmers.

4. Conclusions

We analyse how a micro-swimmer can navigate a complex flow relying only on local hydrodynamic signals. We assume that the swimmer can actively rotate in its frame of reference in response to the local signals. Using reinforcement learning, we found that successful swimming strategies exist only if the swimmer can distinguish the target direction. The flows we considered do not provide direct information concerning the target: the TGV flow has C_4 symmetry and the random velocity field is statistically isotropic. As a consequence, both velocity fields exhibit vertical reflection symmetry. In this case, the dynamics must break vertical reflection symmetry to allow the reinforcement learning algorithm to find meaningful strategies. For example, gravity breaks this symmetry because it causes gyrotaxis or settling and this allows the swimmer to navigate with local signals and actions. For the case of settling owing to gravity, we found that even though settling opposes the migration task, the resulting breaking of vertical reflection symmetry allows the swimmer to swim upwards with an average velocity larger than the settling velocity.

We investigate the underlying mechanism of navigation with local signals by considering swimmers with both gyrotaxis and settling. Reinforcement learning projects out a simple but efficient optimal strategy for vertical navigation: the swimmer measures the strain component, S_{nq}, allowing it to adjust its angular velocity to amplify strain-mediated rotations, which leads to a preferential sampling of strain regions and upwelling regions. For the parameters tested here, we found the same optimal strategy in both the TGV flow and different realisations of a smooth random velocity field, which indicates that the strategy is robust. For the tested cases, the strategy leads to twice the navigation speed compared with a naive gyrotactic swimmer (Kessler 1985; Durham *et al.* 2011, 2013; Gustavsson *et al.* 2016).

In this article, we use a highly idealised model for a micro-swimmer to investigate the role of symmetries in Q-learning using local signals. To speculate in how far the model may apply to any given planktonic micro-organism, the model assumptions must be critically assessed. First, it is assumed that the micro-swimmer is rigid and that the swimmer swims with a constant speed. This rules out jumping copepods escaping predators, but may apply to cruising swimmers. Copepods, for example, can cruise by moving their appendages in specific, high-frequency gaits (Jiang *et al.* 2002). Dinoflagellates can also cruise using their flagella (Kamykowski, Reed & Kirkpatrick 1992). Second, we assume that the micro-swimmer can measure local fluid strain, as well as its relative rotation and its relative translation to the fluid. This is in principle possible with setae or cilia, as for copepods (Kiørboe *et al.* 1999), ciliates (Jakobsen 2001), rotifers (Kirk & Gilbert 1988) and invertebrate larvae (Mackie *et al.* 1976; Fuchs *et al.* 2013). More signals provide more information, facilitating navigation. This suggests that the swimming strategies of a realistic swimmer may rely on all available signals, possibly including light and chemical concentration gradients in addition to hydrodynamic signals. Third, we assume the swimmer is rigid and that hydrodynamic signals are unaffected by the motion of the swimmer. This is because a micro-swimmer is thought to be able to distinguish external fluid disturbance from that generated by its own motion (Hwang & Strickler 2001) by recognising temporal and spatial characteristics of signals (Yen & Strickler 1996; Fields 2014). However, realistic swimmers need to deform smartly to propel (Verma, Novati & Koumoutsakos 2018; Tsang *et al.* 2020; Hartl *et al.* 2021). The interaction between the swimmer and fluid must disturb the local flow field, which makes it more difficult to measure external signals. How and to what extent a swimmer can extract useful signals remain to be investigated. Fourth, our results are obtained for the parameters given in table 1. Although the mechanisms found here are robust to small parameter changes (figure 7 in Appendix A), it is clear that the found strategies must fail when the parameters change substantially. For example, we choose ω_s to be five times larger than the gyrotactic angular velocity of the order of B^{-1}, which facilitates the control of swimming direction. Whether there exist efficient navigation strategies when ω_s is small compared with B^{-1} remains an open question. As another example, for much larger swimming speeds, the preferential sampling becomes weaker (Gustavsson *et al.* 2016), so that it becomes harder to outperform the naive strategy (Colabrese *et al.* 2017).

In our model, we consider steady flows in two spatial dimensions. Our idealised flow configurations allow us to investigate the symmetry problem and the underlying mechanism of hydrodynamic signal in an intuitive way. When generalised to more realistic situations, the breaking of symmetry is also important. For example, symmetry needs to be broken for a swimmer to navigate through locally isotropic turbulence in the ocean. However, the optimal strategies are expected to be different in a three-dimensional and time-dependent flow, because three-dimensional dynamics is more complex and brings additional flow signals to act upon. It remains an open question to determine optimal strategies in three-dimensional unsteady flows. Moreover, in our model, the perceived signals were given by estimated threshold values in table 2, but in reality, the swimmers may respond to other levels of hydrodynamic signals. How can we determine which level is the most important? Is it possible to model the signal under disturbances from swimming?

Optimising the rate of vertical migration is a fairly simple task, and this choice of target allowed us to study the effect of symmetry breaking, and to compare with the existing literature on navigation of smart swimmers (Colabrese *et al.* 2017). However, in nature, there are competing tasks, such as minimising energy consumption during migration or avoiding predation (Huntley & Brooks 1982; Morris, Gust & Torres 1985;

Park *et al.* 2001). How to analyse the effects of these competing tasks remains an open question, necessary to answer to understand observed survival strategies of motile micro-organisms in the ocean.

Funding. K.G. and B.M. are supported in part by a grant from the Knut and Alice Wallenberg Foundation, grant no. 2019.0079, and in part by VR grant no. 2017-3865. K.G. is supported by Vetenskapsrådet, Grant No. 2018-03974. B.M. and L.Z. are supported by a collaboration grant from the joint China–Sweden mobility programme (National Natural Science Foundation of China (NSFC)–Swedish Foundation for International Cooperation in Research and Higher Education (STINT)), grant nos. 11911530141 (NSFC) and CH2018-7737 (STINT). J.Q. and L.Z. acknowledge the support from the Institute for Guo Qiang of Tsinghua University (Grant No. 2019GQG1012). C.X. acknowledges the support from NSFC (Grant No. 91752205).

Declaration of interest. The authors report no conflict of interest.

Author ORCIDs.
Jingran Qiu https://orcid.org/0000-0003-0064-3797;
Kristian Gustavsson https://orcid.org/0000-0002-6613-3821;
Chunxiao Xu https://orcid.org/0000-0001-5292-8052;
Bernhard Mehlig https://orcid.org/0000-0002-3672-6538.

Appendix A. Numerical details

In this appendix, we give details of the different simulations summarised in table 3 and the implementation of the reinforcement learning algorithm.

To implement the Q-learning algorithm, both actions and states are discretised. The action is to modify the angular swimming velocity $\boldsymbol{\omega}_s$ in (2.1*d*). In cases S1, S2, S4, S5 and S6, the actions are given by (2.7). In case S3, the actions are given by (2.8), with $\boldsymbol{k}$ being one of $(0, -1, 0)$, $(1, 0, 0)$, $(0, 1, 0)$ or $(-1, 0, 0)$ (Colabrese *et al.* 2017). The states are given by different combinations of the signals. In cases S1, S3, S4 and S5, the states are given by the combination of S_{nn} and S_{nq}. In case S2, the states are given by the combination of three levels of local vorticity Ω and four discrete levels of the instantaneous direction $\boldsymbol{n}$ of the swimmer (Colabrese *et al.* 2017). In case S6, the states are given either by the signal S_{nq} solely or in combination with one of S_{nn}, Δu_q and $\Delta\Omega$ (see (2.6)).

The training with reinforcement learning is divided into episodes. In each episode, ten swimmers are initialised with random locations and orientations, and simulated to update the Q table in parallel. The Gaussian noises $\boldsymbol{\xi}$ and $\boldsymbol{\eta}$ in (2.1*b*) and (2.1*d*) are implemented at every time step by Gaussian translational and rotational displacements with variances $\sqrt{2D_t\Delta t}$ and $\sqrt{2D_r\Delta t}$, respectively, where $D_t = 0.001L_0u_0$ and $D_r = 0.01u_0/L_0$. For the simulation in the TGV flow, we integrate (2.1) numerically using an explicit second-order Adams–Bashforth scheme for 10^5 time steps of size $\Delta t = 0.01u_0/L_0$, which allows for the position, velocity and orientation of the swimmer to reach a statistically steady state. The state s_i of a given swimmer is evaluated and the Q table is updated every 10 time steps, which results in a total of $i_{max} = 10^4$ state updates in each episode. We use $\gamma = 0.999$, which corresponds to a time window of order $(1-\gamma)^{-1} = 10^3$ state changes or 25 s in physical time. This time window is much longer than the time scale for a swimmer to move through a vortex, estimated by $L_0/v_s = 0.5$ s.

We make similar assumptions and choose similar parameters for our simulations using random velocity fields, but there are a number of minor differences. First, the state s_i is evaluated at every time step but the Q table is updated only when the state changes. Second, each episode lasts for 2500 s, which corresponds to at least $i_{max} = 10^4$ state changes. Third, we use the Euler method to integrate (2.1), rather than the Adams–Bashforth scheme. We confirm that the two approaches yield the same results for the TGV flow.

Flow field	Case	α_0	σ_0	ε_0	j_0	Episode number
TGV flow	S1	0.02	1000	0.0	∞	1000
	S2	0.02	1000	0.0	∞	1000
	S3	0.02	1000	0.0	∞	1000
	S4	0.02	1000	0.0	∞	1000
	S5	0.02	1000	0.0	∞	1000
	S6: S_{nn}, S_{nq}	0.008	1000	0.001	2000	2000
	S6: S_{nq}	0.02	1000	0.0005	1000	1000
	S6: S_{nq}, Δu_q	0.02	1000	0.0005	1000	1000
	S6: S_{nq}, $\Delta\Omega$	0.01	1000	0.001	2000	2000
Random velocity field	S6: all cases	0.04	1000	0.02	2000	3000

Table 4. Training parameters.

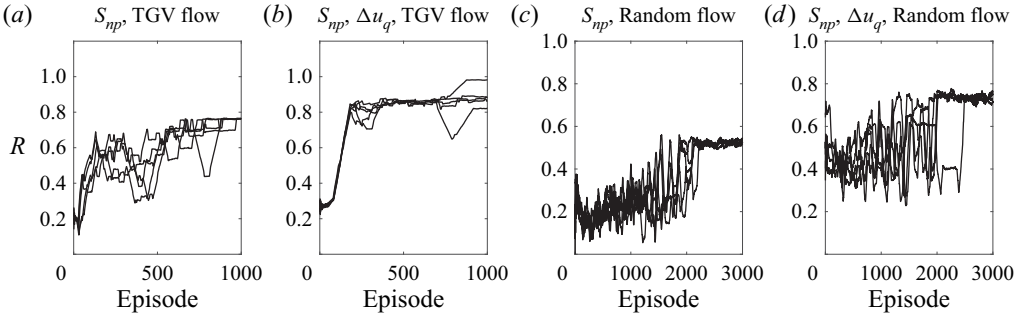

Figure 6. Evolution of the total reward R as a function of episode. The curves represent the moving average of R over 100 episodes. Each panel shows 5 different learning processes.

During training, we take both the learning rate, α, and the exploration rate, ε, to decrease as the episode number j increases, i.e.

$$\alpha = \alpha_0 \frac{\sigma_0}{\sigma_0 + j}, \quad \varepsilon = \varepsilon_0 \max\left(0, 1 - \frac{j}{j_0}\right), \tag{A1a,b}$$

with initial learning and exploration rates α_0 and ε_0 and decay scales σ_0 and j_0. Training parameters for all cases are shown in table 4.

We use the total reward, $R = \sum_{i=0}^{i_{max}} r_i L_0 / T_N v_s$, to evaluate the performance of strategies found during training, where r_i is the reward of each state change defined in (2.9) and i_{max} is the total number of state changes in a single episode. The R indicates how fast a swimmer navigates upward. We note that R is different from the concept of discounted reward, as mentioned in § 2.4. The training has converged when Σ_r has reached a plateau (figure 6).

To test the robustness of the strategies shown in figure 3, we examined the strategies on swimmers whose parameter values are perturbed from table 1. The vertical velocities of swimmers shown in figure 7 show that the optimal strategies are robust to moderate changes of the parameters and better than the naive strategy in most of cases.

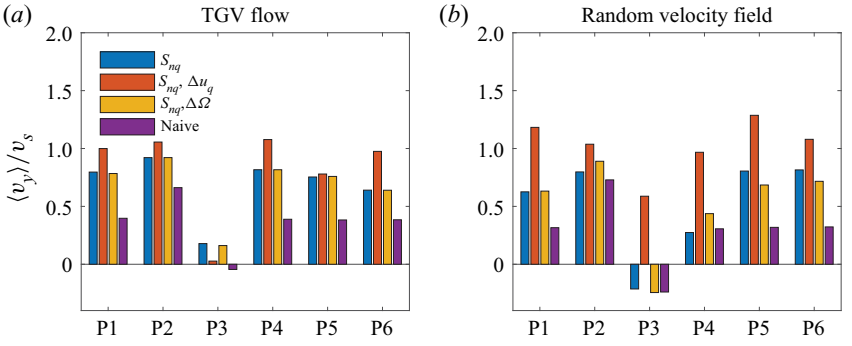

Figure 7. Robustness of strategies to small parameter perturbations. (*a*) TGV flow and (*b*) random velocity field. P1, result for parameters given in table 1. P2, same, but $v_s = 2.0$ mm s^{-1}. P3, $v_s = 0.5$ mm s^{-1}. P4, $\omega_s = 1.2$ rad s^{-1}. P5, $\omega_s = 0.8$ rad s^{-1}. P6, $S_c = 0.8$ s^{-1}.

References

Alageshan, J.K., Verma, A.K., Bec, J. & Pandit, R. 2020 Machine learning strategies for path-planning microswimmers in turbulent flows. *Phys. Rev.* E **101**, 043110.

Barile, P.J., Stoner, A.W. & Young, C.M. 1994 Phototaxis and vertical migration of the queen conch (*Strombus gigas* linne) veliger larvae. *J. Expl Mar. Biol. Ecol.* **183** (2), 147–162.

Biferale, L., Bonaccorso, F., Buzzicotti, M., Di Leoni, P.C. & Gustavsson, K. 2019 Zermelo's problem: optimal point-to-point navigation in 2D turbulent flows using reinforcement learning. *Chaos* **29** (10), 103138.

Bollens, S.M. & Frost, B.W. 1989 Predator-induced diet vertical migration in a planktonic copepod. *J. Plankton Res.* **11** (5), 1047–1065.

Borgnino, M., Boffetta, G., De Lillo, F. & Cencini, M. 2018 Gyrotactic swimmers in turbulence: shape effects and role of the large-scale flow. *J. Fluid Mech.* **856**, R1.

Buskey, E.J., Lenz, P.H. & Hartline, D.K. 2002 Escape behavior of planktonic copepods in response to hydrodynamic disturbances: high speed video analysis. *Mar. Ecol. Prog. Ser.* **235**, 135–146.

Carlotti, F.C.C.O., Bonnet, D. & Halsband-Lenk, C. 2007 Development and growth rates of *Centropages typicus*. *Prog. Oceanogr.* **72** (2-3), 164–194.

Cencini, M., Boffetta, G., Borgnino, M. & De Lillo, F. 2019 Gyrotactic phytoplankton in laminar and turbulent flows: a dynamical systems approach. *Eur. Phys. J.* E **42** (3), 31.

Cohen, J.H. & Forward, R.B. Jr. 2002 Spectral sensitivity of vertically migrating marine copepods. *Biol. Bull.* **203** (3), 307–314.

Cohen, J.H., Last, K.S., Waldie, J. & Pond, D.W. 2019 Loss of buoyancy control in the copepod *Calanus finmarchicus*. *J. Plankton Res.* **41** (5), 787–790.

Colabrese, S., Gustavsson, K., Celani, A. & Biferale, L. 2017 Flow navigation by smart microswimmers via reinforcement learning. *Phys. Rev. Lett.* **118** (15), 158004.

Colabrese, S., Gustavsson, K., Celani, A. & Biferale, L. 2018 Smart inertial particles. *Phys. Rev. Fluids* **3** (8), 084301.

Durham, W.M., Climent, E., Barry, M., De Lillo, F., Boffetta, G., Cencini, M. & Stocker, R. 2013 Turbulence drives microscale patches of motile phytoplankton. *Nat. Commun.* **4**, 2148.

Durham, W.M., Climent, E. & Stocker, R. 2011 Gyrotaxis in a steady vortical flow. *Phys. Rev. Lett.* **106**, 238102.

Durham, W.M., Kessler, J.O. & Stocker, R. 2009 Disruption of vertical motility by shear triggers formation of thin phytoplankton layers. *Science* **323** (5917), 1067–1070.

Fields, D. 2014 The sensory horizon of marine copepods. In *Copepods: Diversity, Habitat and Behavior*, pp. 157–179. Nova Science Publishers, Inc.

Fields, D.M. & Yen, J. 1997 Implications of the feeding current structure of *Euchaeta rimana*, a carnivorous pelagic copepod, on the spatial orientation of their prey. *J. Plankton Res.* **19** (1), 79–95.

Fraga, S. 1989 Chainforming dinoflagellates: an adaptation to red tides. *Red Tides Biol. Environ. Sci. Toxicol.* 281–284.

Frisch, U. 1997 *Turbulence*. Cambridge Univeristy Press.

FUCHS, H.L. & GERBI, G.P. 2016 Seascape-level variation in turbulence-and wave-generated hydrodynamic signals experienced by plankton. *Prog. Oceanogr.* **141**, 109–129.
FUCHS, H.L., GERBI, G.P., HUNTER, E.J., CHRISTMAN, A.J. & DIEZ, F.J. 2015 Hydrodynamic sensing and behavior by oyster larvae in turbulence and waves. *J. Expl Biol.* **218** (9), 1419–1432.
FUCHS, H.L., HUNTER, E.J., SCHMITT, E.L. & GUAZZO, R.A. 2013 Active downward propulsion by oyster larvae in turbulence. *J. Expl Biol.* **216** (8), 1458–1469.
GILBERT, O.M. & BUSKEY, E.J. 2005 Turbulence decreases the hydrodynamic predator sensing ability of the calanoid copepod *Acartia tonsa*. *J. Plankton Res.* **27** (10), 1067–1071.
GUNNARSON, P., MANDRALIS, I., NOVATI, G., KOUMOUTSAKOS, P. & DABIRI, J.O. 2021 Learning efficient navigation in vortical flow fields. arXiv:2102.10536.
GUSTAVSSON, K., BERGLUND, F., JONSSON, P.R. & MEHLIG, B. 2016 Preferential sampling and small-scale clustering of gyrotactic microswimmers in turbulence. *Phys. Rev. Lett.* **116** (10), 108104.
GUSTAVSSON, K., BIFERALE, L., CELANI, A. & COLABRESE, S. 2017 Finding efficient swimming strategies in a three-dimensional chaotic flow by reinforcement learning. *Eur. Phys. J.* E **40** (12), 110.
GUSTAVSSON, K. & MEHLIG, B. 2016 Statistical models for spatial patterns of heavy particles in turbulence. *Adv. Phys.* **61**, 1–57.
HARTL, B., HÜBL, M., KAHL, G. & ZÁŽŮTL, A. 2021 Microswimmers learning chemotaxis with genetic algorithms. *Proc. Natl Acad. Sci.* **118** (19), e2019683118.
HAYS, G.C. 2003 A review of the adaptive significance and ecosystem consequences of zooplankton diel vertical migrations. *Mig. Disp. Mar. Organ.* 163–170.
HUNTLEY, M. & BROOKS, E.R. 1982 Effects of age and food availability on diel vertical migration of *Calanus pacificus*. *Mar. Biol.* **71** (1), 23–31.
HWANG, J.-S. & STRICKLER, R. 2001 Can copepods differentiate prey from predator hydromechanically? *Zool. Stud. Taipei* **40** (1), 1–6.
INCZE, L.S., HEBERT, D., WOLFF, N., OAKEY, N. & DYE, D. 2001 Changes in copepod distributions associated with increased turbulence from wind stress. *Mar. Ecol. Prog. Ser.* **213**, 229–240.
JAKOBSEN, H.H. 2001 Escape response of planktonic protists to fluid mechanical signals. *Mar. Ecol. Prog. Ser.* **214**, 67–78.
JEFFERY, G.B. 1922 The motion of ellipsoidal particles immersed in a viscous fluid. *Proc. R. Soc. Lond. Ser.* A **102**, 161–179.
JIANG, H., OSBORN, T.R. & MENEVEAU, C. 2002 The flow field around a freely swimming copepod in steady motion. Part I: theoretical analysis. *J. Plankton Res.* **24** (3), 167–189.
JIANG, H. & PAFFENHÖFER, G. 2004 Relation of behavior of copepod juveniles to potential predation by omnivorous copepods: an empirical-modeling study. *Mar. Ecol. Prog. Ser.* **278**, 225–239.
KABATA, Z. & HEWITT, G.C. 1971 Locomotory mechanisms in caligidae (crustacea: Copepoda). *J. Fish. Board Canada* **28** (8), 1143–1151.
KAMYKOWSKI, D., REED, R.E. & KIRKPATRICK, G.J. 1992 Comparison of sinking velocity, swimming velocity, rotation and path characteristics among six marine dinoflagellate species. *Mar. Biol.* **113** (2), 319–328.
KESSLER, J.O. 1985 Hydrodynamic focusing of motile algal cells. *Nature* **313**, 218–220.
KIM, S. & KARRILA, S.J. 1991 *Microhydrodynamics: Principles and Selected Applications*. Butterworth-Heinemann.
KIØRBOE, T., ANDERSEN, A., LANGLOIS, V.J. & JAKOBSEN, H.H. 2010 Unsteady motion: escape jumps in planktonic copepods, their kinematics and energetics. *J. R. Soc. Interface* **7** (52), 1591–1602.
KIØRBOE, T., SAIZ, E. & VISSER, A.E. 1999 Hydrodynamic signal perception in the copepod *Acartia tonsa*. *Mar. Ecol. Prog. Ser.* **179**, 97–111.
KIØRBOE, T. & VISSER, A.W. 1999 Predator and prey perception in copepods due to hydromechanical signals. *Acta Obstet. Gyn. Jpn* **179** (3), 81–95.
KIRK, K.L. & GILBERT, J.J. 1988 Escape behavior of polyarthra in response to artificial flow stimuli. *Bull. Mar. Sci.* **43** (3), 551–560.
KNUTSEN, T., MELLE, W. & CALISE, L. 2001 Determining the mass density of marine copepods and their eggs with a critical focus on some of the previously used methods. *J. Plankton Res.* **23** (8), 859–873.
LOVECCHIO, S., CLIMENT, E., STOCKER, R. & DURHAM, W.M. 2019 Chain formation can enhance the vertical migration of phytoplankton through turbulence. *Sci. Adv.* **5** (10), eaaw7879.
MAAR, M., VISSER, A.W., NIELSEN, T.G., STIPS, A. & SAITO, H. 2006 Turbulence and feeding behaviour affect the vertical distributions of *Oithona similis* and *Microsetella norwegica*. *Mar. Ecol. Prog. Ser.* **313**, 157–172.
MACKIE, G.O., SINGLA, C.L. & THIRIOT-QUIEVREUX, C. 1976 Nervous control of ciliary activity in gastropod larvae. *Biol. Bull.* **151** (1), 182–199.

MARTENS, E.A., WADHWA, N., JACOBSEN, N.S., LINDEMANN, C., ANDERSEN, K.H. & VISSER, A. 2015 Size structures sensory hierarchy in ocean life. *Proc. R. Soc.* B*: Biol. Sci.* **282** (1815), 20151346.

MEHLIG, B. 2021 *Machine Learning with Neural Networks*. Cambridge University Press.

MICHALEC, F.C.C.O., SOUISSI, S. & HOLZNER, M. 2015 Turbulence triggers vigorous swimming but hinders motion strategy in planktonic copepods. *J. R. Soc. Interface* **12** (106), 20150158.

MILLERO, F.J., CHEN, C., BRADSHAW, A. & SCHLEICHER, K. 1980 A new high pressure equation of state for seawater. *Deep Sea Res.* A*. Oceanogr. Res. Papers* **27** (3-4), 255–264.

MORRIS, M.J., GUST, G. & TORRES, J.J. 1985 Propulsion efficiency and cost of transport for copepods: a hydromechanical model of crustacean swimming. *Mar. Biol.* **86** (3), 283–295.

MUIÑOS-LANDIN, S., FISCHER, A., HOLUBEC, V. & CICHOS, F. 2021 Reinforcement learning with artificial microswimmers. *Sci. Robot.* **6** (52), eabd9285.

PARK, J.G., JEONG, M.K., LEE, J.A., CHO, K. & KWON, O. 2001 Diurnal vertical migration of a harmful dinoflagellate, Cochlodinium polykrikoides (Dinophyceae), during a red tide in coastal waters of Namhae Island, Korea. *Phycologia* **40** (3), 292–297.

QIU, J., HUANG, W., XU, C. & ZHAO, L. 2020 Swimming strategy of settling elongated micro-swimmers by reinforcement learning. *Sci. China Phys. Mech. Astron.* **63** (8), 284711.

SCHNEIDER, E. & STARK, H. 2019 Optimal steering of a smart active particle. *Europhys. Lett.* **127** (3), 34003.

SENGUPTA, A., CARRARA, F. & STOCKER, R. 2017 Phytoplankton can actively diversify their migration strategy in response to turbulent cues. *Nature* **543** (7646), 555–558.

STRICKLER, J.R. & BAL, A.K. 1973 Setae of the first antennae of the copepod *Cyclops scutifer* (Sars): their structure and importance. *Proc. Natl Acad. Sci.* **70** (9), 2656–2659.

SULLIVAN, J.M., SWIFT, E., DONAGHAY, P.L. & RINES, J.E.B. 2003 Small-scale turbulence affects the division rate and morphology of two red-tide dinoflagellates. *Harmful Algae* **2** (3), 183–199.

SUTTON, R.S. & BARTO, A.G. 1998 *Reinforcement Learning: An Introduction (Adaptive Computation and Machine Learning)*. MIT Press.

TAYLOR, G.I. 1923 VIII. Stability of a viscous liquid contained between two rotating cylinders. *Phil. Trans. R. Soc. Lond. Ser.* A*, Contain. Pap. Math. Phys. Character* **223** (605-615), 289–343.

TITELMAN, J. 2001 Swimming and escape behavior of copepod nauplii: implications for predator-prey interactions among copepods. *Mar. Ecol. Prog. Ser.* **213**, 203–213.

TITELMAN, J. & KIØRBOE, T. 2003 Motility of copepod nauplii and implications for food encounter. *Mar. Ecol. Prog. Ser.* **247**, 123–135.

TSANG, A.C.H., TONG, P.W., NALLAN, S. & PAK, O.S. 2020 Self-learning how to swim at low Reynolds number. *Phys. Rev. Fluids* **5** (7), 074101.

VERMA, S., NOVATI, G. & KOUMOUTSAKOS, P. 2018 Efficient collective swimming by harnessing vortices through deep reinforcement learning. *Proc. Natl Acad. Sci.* **115** (23), 5849–5854.

VISSER, A. 2010 *Small, Wet & Rational: Individual Based Zooplankton Ecology*. Technical University of Denmark.

VISSER, A.W. 2001 Hydromechanical signals in the plankton. *Mar. Ecol. Prog. Ser.* **222**, 1–24.

WATKINS, C.J.C.H. & DAYAN, P. 1992 Q-learning. *Mach. Learn.* **8** (3), 279–292.

YAMAZAKI, H. & SQUIRES, K.D. 1996 Comparison of oceanic turbulence and copepod swimming. *Mar. Ecol.-Prog. Ser.* **144**, 299–301.

YEN, J., LENZ, P.H., GASSIE, D.V. & HARTLINE, D.K. 1992 Mechanoreception in marine copepods: electrophysiological studies on the first antennae. *J. Plankton Res.* **14** (4), 495–512.

YEN, J. & STRICKLER, J.R. 1996 Advertisement and concealment in the plankton: what makes a copepod hydrodynamically conspicuous? *Invertebr. Biol.* 191–205.

ZHAO, L., CHALLABOTLA, N.R., ANDERSSON, H.I. & VARIANO, E.A. 2015 Rotation of nonspherical particles in turbulent channel flow. *Phys. Rev. Lett.* **115** (24), 244501.

ZHAO, L., GUSTAVSSON, K., NI, R., KRAMEL, S., VOTH, G.A., ANDERSSON, H.I. & MEHLIG, B. 2019 Passive directors in turbulence. *Phys. Rev. Fluids* **4**, 054602.